Environmental Pollution 349 (2024) 123997

Contents lists available at ScienceDirect

Environmental Pollution

journal homepage: www.elsevier.com/locate/envpol

Assessing the impact of COVID-19 era drug combinations on hepatic functionality: A thorough investigation in adult *Danio rerio*☆

Diana Belen Onofre-Camarena [a], Gustavo Axel Elizalde-Velázquez [a], Leobardo Manuel Gómez-Oliván [a,*], Sandra García-Medina [b], Marcela Galar-Martínez [b], José Roberto Jerónimo Juárez [a], Selene Elizabeth Herrera-Vázquez [a]

[a] *Laboratorio de Toxicología Ambiental, Facultad de Química, Universidad Autónoma del Estado de México, Paseo Colón Intersección Paseo Tollocan, Colonia Residencial Colón, CP, 50120, Toluca, Estado de México, Mexico*

[b] *Laboratorio de Toxicología Acuática, Departamento de Farmacia, Escuela Nacional de Ciencias Biológicas, Instituto Politécnico Nacional. Unidad Profesional Adolfo López Mateos, Av. Wilfrido Massieu s/n y cerrada Manuel Stampa, Col. Industrial Vallejo, Ciudad de México, CP, 07700, Mexico*

ARTICLE INFO

Keywords:
COVID-19 drugs
Oxidative damage
Histological damage
Gene expression
Zebrafish

ABSTRACT

Current and thorough information on the ecotoxicological consequences of pharmaceuticals is accessible globally. However, there remains a substantial gap in knowledge concerning the potentially toxic effects of COVID-19 used drugs, individually and combined, on aquatic organisms. Given the factors above, our investigation assumes pivotal importance in elucidating whether or not paracetamol, dexamethasone, metformin, and their tertiary mixtures might prompt histological impairment, oxidative stress, and apoptosis in the liver of zebrafish. The findings indicated that all treatments, except paracetamol, augmented the antioxidant activity of superoxide dismutase (SOD) and catalase (CAD), along with elevating the levels of oxidative biomarkers such as lipid peroxidation (LPX), hydroperoxides (HPC), and protein carbonyl content (PCC). Paracetamol prompted a reduction in the activities SOD and CAT and exhibited the most pronounced toxic response when compared to the other treatments. The gene expression patterns paralleled those of oxidative stress, with all treatments demonstrating overexpression of *bax*, *bcl2*, and *p53*. The above suggested a probable apoptotic response in the liver of the fish. Nevertheless, our histological examinations revealed that none of the treatments induced an apoptotic or inflammatory response in the hepatocytes. Instead, the observed tissue alterations encompassed leukocyte infiltration, sinusoidal dilatation, pyknosis, fatty degeneration, diffuse congestion, and vacuolization. In summary, the hepatic toxicity elicited by COVID-19 drugs in zebrafish was less pronounced than anticipated. This attenuation could be attributed to metformin's antioxidant and hormetic effects.

1. Introduction

The advent of the COVID-19 pandemic on March 11, 2020, marked a profound turning point worldwide, ushering in a multifaceted landscape that intertwined health, economy, politics, society, and the environment. In the domain of health, the widespread prevalence of COVID-19 led to the extensive use of various pharmaceuticals such as paracetamol, dexamethasone, and metformin (Micallef et al., 2020; Stasi et al., 2020; Ala and Ala, 2021). Paracetamol was widely used to alleviate symptoms such as fever, muscle fatigue, and pain (Graham et al., 2013; Stasi et al., 2020). Likewise, dexamethasone significantly reduced lung inflammation among critically ill patients (RECOVERY Collaborative Group, 2021). Additionally, metformin emerged as a critical medication, reducing mortality rates in patients with type 2 diabetes who contracted COVID-19 and followed this treatment regimen (Lukito et al., 2020). Notably, these drugs, integral to the fight against COVID-19, are also fundamental in treating diverse ailments. Consequently, there was a substantial rise in the production and consumption of these medications, as evidenced by the significant increase in the total sales of each drug. Before the onset of COVID-19 in 2020, dexamethasone's global sales amounted to $500 million. Post-COVID-19, by the end of 2022, these figures surged to $1052 million, illustrating a remarkable growth trajectory. Similarly, paracetamol saw a rise in sales from $821.23 million in 2021 to $940.79 million in 2023, albeit at a more moderate pace than

☆ This paper has been recommended for acceptance by Dr Jiayin Dai.

* Corresponding author.
E-mail addresses: lmgomezo@uaemex.mx, lgolivan74@gmail.com (L.M. Gómez-Oliván).

https://doi.org/10.1016/j.envpol.2024.123997
Received 29 February 2024; Received in revised form 3 April 2024; Accepted 15 April 2024
Available online 16 April 2024

dexamethasone. Metformin, with global sales of $258.40 million in 2021, experienced an increase to $342.3 million in 2023. While all three drugs exhibited growth in the post-COVID-19 period, dexamethasone showed the most significant surge, followed by metformin and then paracetamol. These shifts likely reflect heightened demand for specific medications during and after the pandemic and changes in healthcare policies and consumer behavior.

A surge in the utilization of these pharmaceutical compounds may culminate in a commensurate escalation in their prevalence within water bodies, owing to the suboptimal removal rates observed in wastewater treatment plants (Greenham et al., 2019; Hayden et al., 2022; Liu et al., 2023). Even though there was no follow-up of these pharmaceutical substances within aquatic ecosystems throughout the COVID-19 period, it is essential to underscore that these compounds in surface water have been documented globally (aus der Beek et al., 2016; Praveena et al., 2018; Burns et al., 2018; Rivera-Jaimes et al., 2018; Abdallah et al., 2019; Desgens-Martin and Keller, 2021; Pulicharla et al., 2021; Zhang et al., 2021; Mastrángelo et al., 2022; Wilkinson et al., 2022). For instance, aus der Beek et al., 2016 repor ted that in Brazil, particularly in the Ceará River, a concentration of 589 μg/L of dexamethasone (DEX) was identified. Furthermore, in China, values ranging from 0.002 to 0.050 μg/L have been documented in the Wenyu, Qing, Ba, and Tonghui Rivers in Beijing, as well as in the Pearl River, where a concentration of 0.00033 μg/L was identified (Gong et al., 2019; Shen et al., 2020). On a different note, Mastrángelo et al., 2021 documented the highest recorded concentration of paracetamol in South America, measuring 9.62 μg/L in the surface water of Argentina. Nevertheless, higher concentrations have been reported by other researchers on different continents. As an illustration, Angeles et al. (2020); Ogunbanwo et al., 2022 described the presence of PCM in the surface water of Bangladesh and Nigeria at concentrations of 43.518 μg/L and 111 μg/L, respectively. Finally, as per the findings of Wilkinson et al. (2022), the highest documented concentration of metformin (MET) in the Americas was 64,100 μg/L, identified in the surface waters of Bolivia.

Extensive research findings have consistently demonstrated the profound impact of drug presence in aquatic environments on aquatic organisms' health and overall well-being. MET, PCM, and DEX, for instance, have been conclusively linked to inducing detrimental effects such as oxidative stress, embryotoxicity, behavioral alterations, and other harmful consequences (Sharma et al., 2019; Rosas-Ramírez et al., 2022; Gutiérrez-Noya et al., 2023; Elizalde-Velázquez et al., 2023). Nevertheless, it is crucial to note that only a limited number of studies have so far concentrated on examining the toxic effects generated by drug mixtures. Considering those above, our study holds paramount significance in comprehending and addressing the following inquiries: (1) Can dexamethasone, paracetamol, and metformin at environmentally relevant concentrations induce histological damage in the liver of zebrafish? (2) Will the tertiary mixtures of the abovementioned compounds produce a synergistic or additive effect? and (3) Do the compounds mentioned above cause histological damage through mechanisms involving oxidative stress and apoptosis? Bearing in mind the potential liver toxicity induced by these individual compounds, it is hypothesized that tertiary mixtures will have a more pronounced adverse impact on the liver compared to the compounds administered individually.

2. Method

2.1. Reagents

The reference standards of paracetamol (PCM) (CAS number: 103-90-2) and dexamethasone (DEX) (CAS number: 50-02-2) were obtained from Sigma-Aldrich (St. Louis, MO). Meanwhile, metformin hydrochloride (MET) (CAS number: 1115-70-4) was acquired from Toronto Chemical Research (Toronto, Ontario). The stock solutions of PCM and MET were prepared using distilled water, and only the stock solution of DEX was dissolved in dimethyl sulfoxide (DMSO at 0.01%) due to its low solubility, as Jacob et al. (2018) reported.

2.2. Zebrafish husbandry

Adult male and female *Danio rerio* of the AB strain were utilized for this research project. These specimens were housed in 100-liter aquariums, ratio 1fish/L, filled with dechlorinated and UV-filtered water maintained at specific conditions (temperature: 27 ± 1.5 °C, pH: 7.2–7.6, with a light-dark cycle of 14:10). Water changes were conducted every three days, and the fish were fed twice daily with commercial flakes (LOMAS® Basic Flakes for Tropical Fish) containing 44% protein, 10% fat, 2% fiber, 6% moisture, 12% ash, and 26% nitrogen-free extract.

2.3. Zebrafish exposure

Four hundred adult fish were allocated across sixteen systems, each containing 30 L of dechlorinated and UV-filtered water (25 fish per system). Two of these systems were assigned to the control and DMSO groups. Meanwhile, the remaining fourteen systems were employed to expose fish to the individual drugs and their respective combinations (Table 1). The exposure period lasted 96 h, during which the water was refreshed daily.

2.4. Organ collection

Upon completing the designated exposure period of 96 h, no deceased fish were recorded within the control and DMSO groups. Contrastingly, in all other experimental systems, an average of 2 fish (standard deviation ± 1) were found to be deceased. Consequently, twenty-two fish were utilized for the subsequent analyses involving oxidative stress quantification, gene expression assessment, and histopathological examinations. This way, ten fish were employed for each study in the initial two tests. Meanwhile, a more restricted sample size was utilized for histopathological analyses, involving only two fish for the examination process. All fish were euthanized through hypothermic shock. Subsequently, a precise longitudinal incision was made in the thoracic region using surgical scissors. Following the incision, a thorough dissection was performed with dissecting forceps to remove the liver from each specimen. The extracted organs were transferred into Eppendorf tubes. The tubes for quantifying oxidative stress were filled with 1 mL of phosphate-buffered saline solution with a pH of 7.4 (referred to as PBS 7.4). In contrast, the tubes for evaluating gene expression and conducting histopathological examinations were filled with RNALater (Thermo Fisher Scientific) and formalin, respectively.

Table 1
Exposure systems for *Danio rerio* adults.

Systems		Drugs		
		DEX (ng/L)	PCM (μg/L)	MET (μg/L)
1	COTROL	–	–	–
2	DMSO 0.01%	–	–	–
3	DEX1	30	–	–
4	DEX2	60	–	–
5	PCM1	–	0.250	–
6	PCM2	–	0.500	–
7	MET1	–	–	20
8	MET2	–	–	40
9	DPM1	30	0.250	20
10	DPM2	60	0.250	20
11	DPM3	30	0.250	40
12	DPM4	60	0.250	40
13	DPM5	30	0.500	20
14	DPM6	60	0.500	20
15	DPM7	30	0.500	40
16	DPM8	60	0.500	40

The tubes were carefully stored at a controlled temperature ranging from 2 °C to 4 °C until further analysis. Per the manufacturer's guidelines (Thermo Fisher Scientific), the RNA Later AM7024 solution is designed to maintain sample integrity for one month when stored at 4 °C. Nonetheless, all samples underwent processing within the initial 96-h period.

2.5. Oxidative stress quantification

The tissue was homogenized using a rotor-stator homogenizer. Subsequently, two tubes were obtained from each homogenized sample. The first of these tubes was prepared by combining 300 μL of homogenate with 300 μL of 20% trichloroacetic acid and centrifuged at 11495 rpm at 4.0 °C for 15 min. The precipitate from this tube was utilized to quantify carbonylated proteins (PCC) content following the methodology outlined by Levine et al. (1994). Moreover, the supernatant was employed to measure the degree of lipoperoxidation (LPO) and the levels of hydroperoxides (HPC) based on the procedure described by Buege and Aust (1978) and the work of Jiang et al. (1992) respectively. To prepare tube 2, 700 μL of homogenate was centrifuged at 12,500 rpm at 4.0 °C for 15 min. The supernatant from this tube was utilized for the determination of superoxide dismutase (SOD) and catalase, as outlined by Misra and Fridovich (1972) and Radi et al. (1991), respectively. The results obtained from all biomarkers were standardized using the Bradford method, Bradford (1976).

2.6. Gene expression evaluation

The RNA isolation procedure was conducted within a controlled environment provided by a laminar flow hood (Bioevopeak, China). This hood maintained positive pressure to prevent the ingress of environmental contaminants. The samples were thawed meticulously in an ice bath to initiate the process. Subsequently, each tissue sample underwent the RNA isolation protocol using the RNeasy Mini Kit from QIAGEN. The quality of the isolated RNA was assessed using agarose gel electrophoresis (1%), while its purity was determined through spectrophotometry (NanoDrop, 2000/2000c Thermo Scientific, USA). The extracted RNA was stored at −20 °C until further use. The RNA samples were thawed in an ice bath before reverse transcription. In a sterile Eppendorf tube devoid of RNases, 2.0 μL of 7x gDNA Wipeout Buffer (from the QuantiTect Reverse Transcription Kit by QIAGEN), 10.0 μL of the RNA template, and 2.0 μL of RNase-free water (also from the QuantiTect Reverse Transcription Kit by QIAGEN) were combined. This mixture was incubated for 2 min at 42 °C and promptly cooled on ice. Subsequently, 1.0 μL of Quantiscript reverse transcriptase, 4.0 μL of Quantiscript RT Buffer 5 ×, and 1.0 μL of RT Primer Mix (all components from the QuantiTect Reverse Transcription Kit by QIAGEN) were added to the cooled mixture. The components above were combined and subjected to incubation at a temperature of 42 °C for 15 s, followed by a subsequent incubation at 93 °C for 3 min to facilitate reverse transcription inactivation. Following the completion of the reverse transcription process, the quality of the resulting complementary DNA (cDNA) was meticulously assessed through methods involving electrophoresis and spectrophotometry, as previously delineated. The qPCR reaction was performed by adding 25 μL of the 2 × QuantiTect SYBR Green PCR (QIAGEN), 1.0 μL of each primer, 4.0 μL of cDNA, and 19 μL of RNase-free water. The genes evaluated are shown in Table 2. All reagents were mixed, and the qPCR was run using these conditions: 94 °C for 10 min, followed by 35 cycles of denaturation 94 °C for 15 s, primer annealing for 30 s, and extension 72 °C for 30 s. The Gene Q Rotor (QIAGEN) was employed as the qPCR equipment. The β-actin gene was utilized to normalize the expression of target genes. The $2^{-\Delta\Delta Cq}$ method (Pfaffl, 2001; Pfaffl et al., 2002; Schmittgen and Livak, 2008) was applied to calculate mRNA expression changes. Upon completion of the qPCR amplification cycles, a dissociation curve analysis was conducted under the following parameters: a preliminary denaturation step at 95 °C for 10 s, followed by a temperature reduction to 65 °C for 10 s, and subsequent re-elevation to 95 °C for 10 s, with increments of 0.2 °C. This meticulous procedure served to discern specific from non-specific products within the samples. Data points were collected at each increment of the melting curve. Negative controls were incorporated to confirm the validity of the results, utilizing samples devoid of template, with RNase-free water serving as the substitute.

Table 2
Nucleotide sequences of the primers designed for the (qRT-PCR) analysis.

Gen	Access Number	Forward, Reverse	Primer Sequence (5'→3')
bax	AF231015	F	GGC TAT TTC AAC CAG GGT TCC
		R	TGC GAA TCA CCA ATG CTG T
bcl2a	NM_001030253	F	TAC GGG ATG CTG GAG ATG AA
		R	CCC AGT TCA CTC CGT CTC TA
p53	NM_001271820	F	GCG GAT TTG CTT TGT GGA TG
		R	CCG ACC TCC TCT CCA CTA AA
nrf1a	NM_001328540.1	F	CAG TGA CAG TAG CCC AGG TG
		R	CTG ACG CTT GTG TGG TTT GG
nrf2a	NM_182889.1	F	GGC GAT CCT CCT GTA AAC CC
		R	CCG AAG GAT CCG TCT TCG GT

2.7. Histopathological examinations

Two liver samples per treatment group were placed individually and horizontally into tissue cassettes of the SIMPORT Histosette type. These samples were then subjected to fixation utilizing a Davidson solution, as detailed by Miki et al., in 2018. After 15 days of fixation, the livers underwent decalcification in a 5% hydrochloric acid solution for one week. Subsequently, they were systematically dehydrated, cleared, and infiltrated with alcohols of varying concentrations and xylene before being finally embedded in paraffin. Employing a rotary microtome (CUT 5062 SLEE), these samples were subsequently sectioned to a uniform thickness of 5 μm. The histological sections were meticulously collected in a temperature-controlled water bath, maintained at 37 °C, using the Slidetec Water/Hea SLEE equipment, and were then transferred to clean glass slides. These glass slides were subsequently subjected to an oven at a temperature of 50 °C to facilitate the melting of the paraffin embedded within the samples. The next step involved staining all slides. This staining procedure entailed immersing the slides in a solution of hematoxylin for 30 min, followed by a 10-min immersion in eosin. Subsequently, these stained slides were covered with a solution comprising xylol and resin. For the subsequent histopathological analysis, the samples were diligently examined using an optical microscope of the ZEISS Primo Star model, coupled with a digital camera, the CANON Powershot G10, and a laptop from TOSHIBA, model Satellite. Photomicrographs were captured with the assistance of the software CANON Utilities Remote Capture DC 3.1.0.5 and then edited using the software ZEISS AxiS 40 V 4.8.0.0.

2.8. Drug quantification

The extraction process involved a straightforward liquid extraction procedure. Initially, the fortified samples were homogenized, followed by the addition of specific quantities of formic acid (1%), methanol (0.25 mL), and acetonitrile (0.25 mL). Subsequently, the glass tubes containing the samples underwent rigorous agitation through vortex and vertical shaking for 10 min. Post agitation, the tubes were centrifuged at 10,000 rpm for 12 min. This procedure was repeated, and the supernatant from each extraction was meticulously collected into separate glass tubes. Following the extraction process, the solvent was meticulously evaporated to dryness using an Eppendorf concentrator plus, maintained at a temperature of 45 °C. The resultant powder

obtained from the vacuum was then reconstituted by combining it with 1 mL of n-hexane and 0.5 mL of the mobile phase. This reconstituted mixture was subjected to vortexing, defatting, and subsequent centrifugation at 10,000 rpm for 5 min. The bottom layer was meticulously filtered through a 0.22 μm nylon membrane filter. Subsequently, 10.0 μL of the filtered liquid was injected under optimized conditions for further analysis. The meticulous separation of DEX (50 mm × 3.0 mm, 2.7 μm), PCM (2.1 mm × 100 mm, 1.7 μm), and MET (50 mm × 3.0 mm, 3.5 μm) through chromatography was conducted using specific columns tailored to each compound. DEX was processed through a UPLC BEH column, PCM underwent separation via a reversed-phase C18 column, and MET was meticulously separated using an Xbridge C18 column. For the quantification of PCM, the mobile phase consisted of a mixture of formic acid in water (0.1%) and formic acid in methanol (0.1%) in a ratio of 20:80. In the case of DEX, the mobile phases included 0.1% (v/v) formic acid in water (A) and 0.1% (v/v) formic acid in methanol (B). Additionally, for the determination of MET, eluent A in the mobile phase contained 2.0 mM $MeCOO^-$, while mobile phase B was composed of 100% acetonitrile. Data acquisition and processing were carried out using the Analyst 1.6 software. The accuracy of the proposed process was set by the control spiking method, which we carried out by spiking drug-free liver tissue homogenates with PCM and CPX at three singular percentages (80%, 100%, and 120%). The precision of the established procedure was determined through the control spiking method. This method involved enriching liver tissue homogenates devoid of drugs with PCM, DEX, and MET at specific concentrations (80%, 100%, and 120%) to ensure accurate calibration.

2.9. Statistical analysis

Bartlett tests were utilized to confirm homoscedasticity, while normality was assessed through the Shapiro-Wilk test. Differences in means were determined using the Tukey test, with a significance level set at $p < 0.05$. Differences between treatment groups were examined using a one-way ANOVA test at a significance level of $\alpha = 0.05$ (Sigma Plot 12.3 software). Results from all experiments were presented as the mean ± standard deviation (SD). A Pearson correlation analysis was conducted to assess the strength of association among oxidative stress, gene expression, and histopathological outcomes, with a predetermined significance level of $p < 0.05$. Subsequently, the obtained correlation was visually depicted through a weighted network.

3. Results

3.1. Oxidative stress

Antioxidant activity of SOD and CAT in *Danio rerio* liver demonstrated a concentration-dependent increase in all treatments, but PCM, after 96 h of exposure (Fig. 1 A-B). PCM showcased the exclusive capability to significantly reduce the activity of the above enzymes at its highest concentration compared to its lowest concentration. Even though mixtures displayed a concentration-dependent increase in the antioxidant activity of SOD and CAT, it is paramount to indicate values from DPM1 to DPM6 were below the ones of individual drugs. Similar to the antioxidant activity of superoxide dismutase (SOD) and catalase (CAT), the biomarkers indicative of oxidative damage manifested a

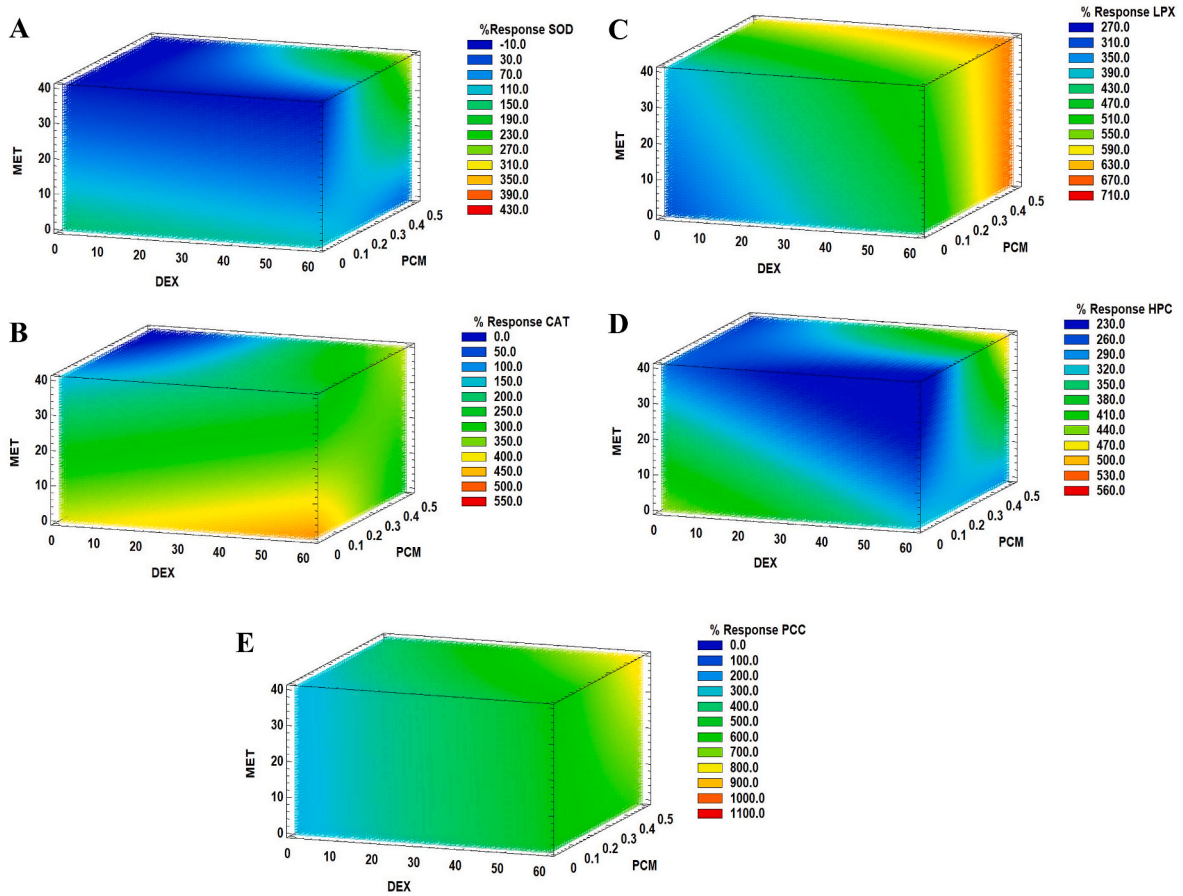

Fig. 1. Oxidative stress elicited by COVID-19 drugs (DEX, PCM, MET) within the liver of *Danio rerio*. Asterisks (*) indicate a significant difference compared to the control group. The presented data depict the mean values ± standard deviation derived from three distinct experiments. Letteres correspond to each of oxidative stress biomarkers (**A**: SOD, **B**: CAT, **C**: LPX, **D**: HPC, **E**: PCC).

significant and concentration-dependent elevation across all treatments compared to the control group (Fig. 1C–E). PCM demonstrated the most pronounced surge in oxidative damage biomarkers, followed by DPM6, DPM7, and DPM8. DPM1 to DPM5 mixtures exhibited an augment similar to the one produced by drugs MET and DEX.

3.2. Gene expression

All treatments, but DMSO, significantly up-regulated the expression of all genes related to apoptosis (*p53*, *bax*, and *bcl2*) and antioxidant activities (*nrf1* and *nrf2*) in *Danio rerio* liver (Fig. 2). Nonetheless, differences were observed among the distinct treatments. As an illustration, the mixtures exhibited the most conspicuous expression of all genes compared to the various treatments. Moreover, it is noteworthy to indicate that individual drugs (PCM, MET, and DEX) showed a more notorious expression of *p53* and *nrf2*; meanwhile, the mixtures DPM1 to DPM4 and DPM 6 exhibited a more pronounced expression of *bax*. *p53*, *nrf1,* and nrf2 were the most up-regulated genes in mixtures DPM5, DPM7, and DPM8, respectively.

3.3. Histopathological damage

Different tissue alterations were observed across all treatments. Tissue alterations identified in *Danio rerio* liver encompassed pyknosis, leukocyte infiltration, fatty degeneration, diffuse congestion, sinusoidal dilatation, and vacuolization (Fig. 3A–P). As depicted in Table 3, mixtures exhibited the most significant occurrence of tissue modifications in *Danio rerio*'s liver. The sole deviation from this pattern was noted in the case of DPM3 (K), wherein the incidence rate closely resembled that observed with individual drugs. Leukocyte infiltration demonstrated the highest frequency among tissue alterations, succeeded by vacuolization and sinusoidal dilatation (see Fig. 4).

3.4. Drug quantification

The concentrations of MET, DEX, and PCM remained below the limit of quantification in the liver of fish exposed to the control group and DMSO. For individual drugs, the compounds not intentionally introduced into the water were consistently found to be below the limit of quantification in the fish's liver. Conversely, mixtures revealed the presence of all three drugs in the fish's liver. Overall, there was a positive correlation between the nominal concentration in water and the corresponding concentration of drugs in *Danio rerio*'s liver, indicating an increase as the nominal concentration elevated (Table 4).

3.5. Pearson correlation

Our weighted network analysis revealed a strong correlation among oxidative damage biomarkers (LPX, HPC, and PCC), tissue alterations (P), and the expression levels of genes associated with antioxidant (*nrf1* and *nrf2*) and apoptotic (*bax*, *bcl2*, and *p53*) responses. Conversely, SOD and CAT exhibited a strong positive correlation with each other; nevertheless, these biomarkers also demonstrated a moderate to strong correlation with oxidative damage biomarkers and tissue alterations but a weak correlation with the expression levels of *nrf1*, *nrf2*, *bax*, *bcl2*, and *p53* genes.

4. Discussion

Up to date, comprehensive data on the ecotoxicological impact of pharmaceuticals are available globally. Nevertheless, a significant knowledge deficit persists regarding 1) the likely toxic effects of drugs used in treating COVID-19 on aquatic organisms and 2) the repercussions and influences that intricate combinations of these substances may exert on these organisms. In light of the preceding information, this investigation explored the potentially toxic effects of MET, PCM, DEX, and their mixtures within the liver of *Danio rerio*. Based on our findings, each drug (PCM, DEX, and MET), both in isolation and when combined, elicited an oxidative stress response in the hepatic tissue of the fish under investigation. Overall, these outcomes align with previously documented findings. For instance, Perussolo et al. (2019) described that the exposure of *Rhamdia quelen* to concentrations of 0.25, 2.5, and 25 μg/L of PCM led to elevated levels of LPX and a simultaneous decline in the antioxidant activity of SOD, glutathione S-transferase (GST), and reduced glutathione (GSH) following 14-day exposure period. Likewise, Elizalde-Velázquez et al., 2023 demonstrated that environmentally relevant concentrations of MET (20 and 40 μg/L) induced oxidative stress in the liver of *Danio rerio*, resulting in impaired liver function in these organisms. Moreover, Pes et al., 2022 conducted an investigation involving *Solea senegalensis*, elucidating that the short-term exposure (7 days) of this fish to DEX resulted in heightened liver glycogen content and modifications to the antioxidant status of SOD and glutathione peroxidase (GPX). Even though, herein, mixtures also showed an increase in the antioxidant activity of SOD and CAT, this

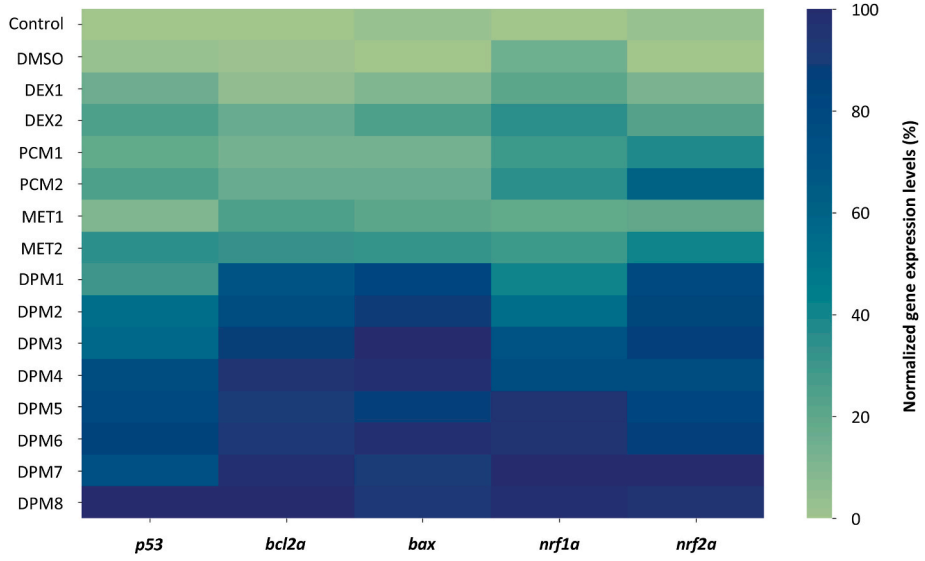

Fig. 2. Normalized expression levels of genes associated with apoptosis (*p53*, *blc2*, *bax*) and antioxidant activity (*nrf1* and *nrf2*) following acute exposure of *Danio rerio* to COVID-19 drugs (DEX, PCM, and MET). The presented data depict the mean values ± standard deviation derived from three distinct experiments.

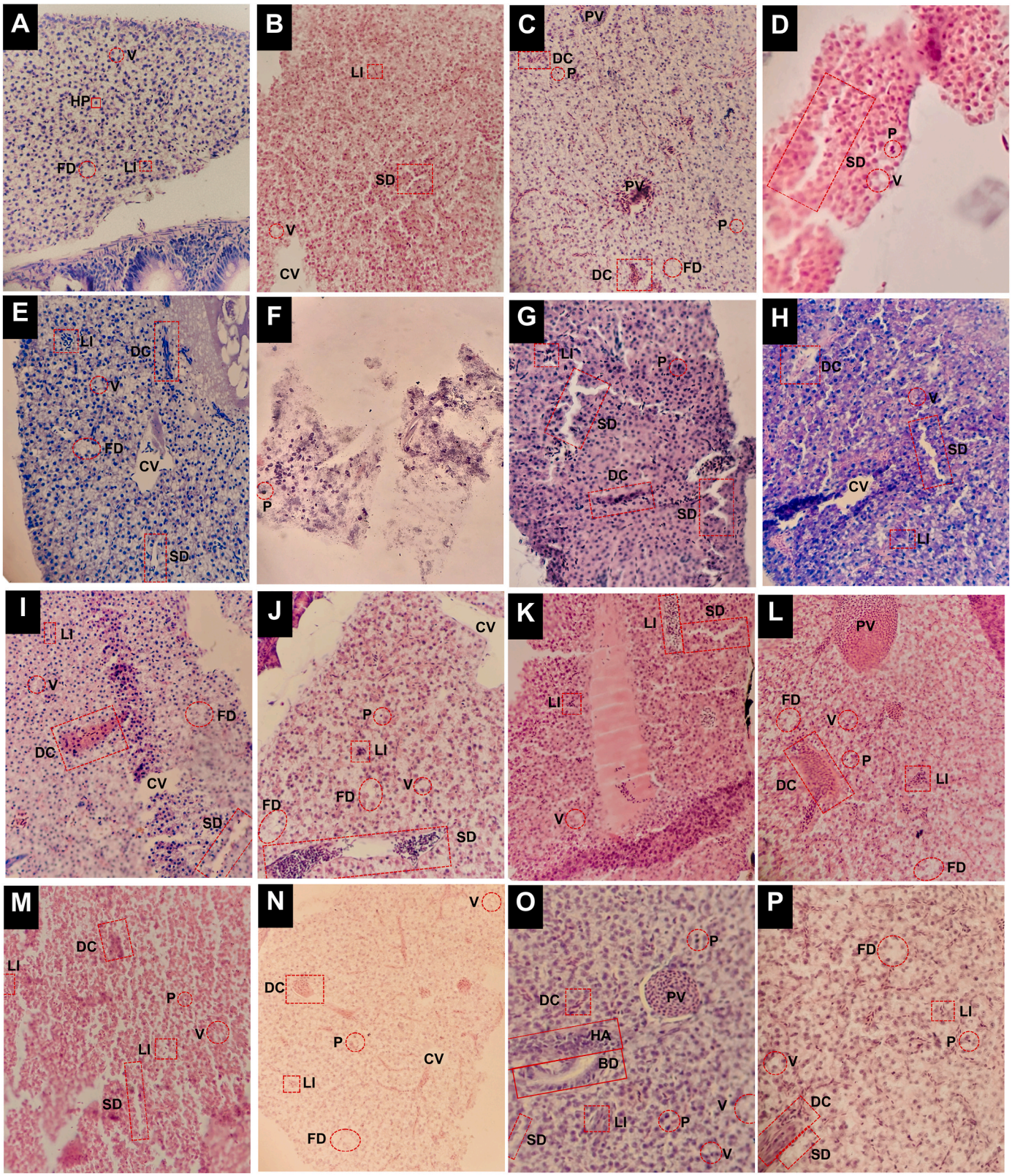

Fig. 3. Histopathological analysis of the zebrafish (*Danio rerio*) liver after acute exposure to DEX, PCM, MET, and their respective combinations. **HA**: hepatic artery, **HP:** hepatocyte, **BD:** bile duct, **CV:** central vein, **PV:** portal vein. Pathological changes are indicated as follows: **Arrow:** pyknosis, **Rectangle:** leukocytic infiltration, **Parallelogram:** fatty degeneration, **Pentagon:** diffuse congestion, **Hexagon:** sinusoidal dilation, **Circle:** vacuolization. **A.** Control. **B.** DMSO 0.01%. **C:** 0.250 μg/L PCM. **D:** 0.500 μg/L PCM. **E.** 30 ng/L DEX. **F.** 60 ng/L DEX. **G.** 20 μg/L MET. **H.** 40 μg/L MET. **I.** 0.250 μg/L PCM, 30 ng/L DEX, 20 μg/L MET. **J.** 0.250 μg/L PCM, 60 ng/L DEX, 20 μg/L MET. **K.** 0.250 μg/L PCM, 30 ng/L DEX, 40 μg/L MET. **L.** 0.250 μg/L PCM, 60 ng/L DEX, 40 μg/L MET. **M.** 0.500 μg/L PCM, 30 ng/L DEX, 20 μg/L MET. **N.** 0.500 μg/L PCM, 60 ng/L DEX, 20 μg/L MET. **O.** 0.500 μg/L PCM, 30 ng/L DEX, 40 μg/L MET. **P.** 0.500 μg/L PCM, 60 ng/L DEX, 40 μg/L MET. Hematoxylin and eosin staining. Observations were made at a magnification of 40×.

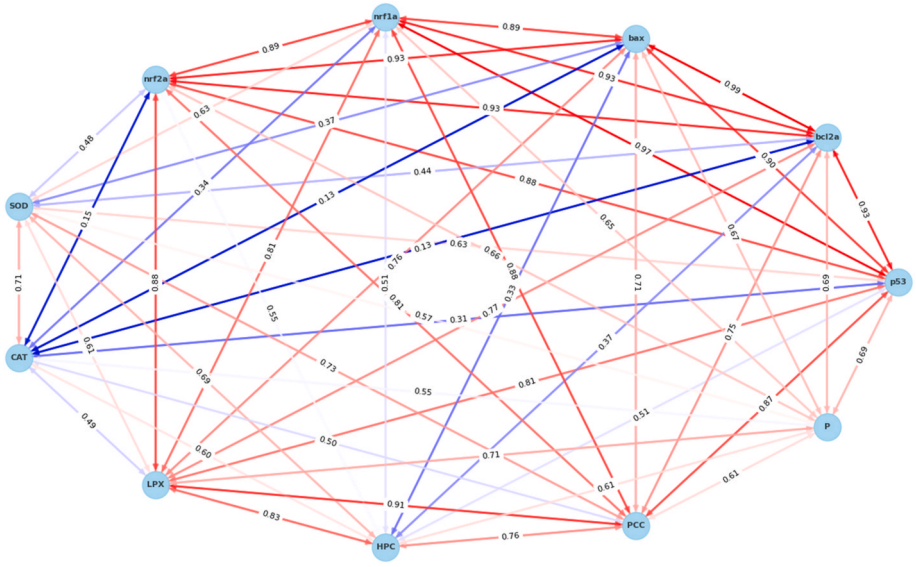

Fig. 4. Pearson correlation among studied variables (oxidative stress, gene expression, and histopathological (P) outcomes). The figure depicts a weighted network, where each arrow symbolizes a connection between nodes (variables) and is assigned a numerical value known as a weight. These weights capture the strength or significance of the relationships between nodes and can vary from positive to negative, depending on the nature of the relationship being depicted. Given the positive correlation among all variables, arrows within the weighted network were distinguished by red and blue colors. The intensity of color in the arrows of the weighted network corresponds directly to the strength of the positive correlation between biomarkers, with a higher positive correlation yielding a more vivid red hue. In contrast, a bluer shade in the arrows represents a lower positive correlation. (For interpretation of the references to color in this figure legend, the reader is referred to the Web version of this article.)

Table 3
Prevalence matrix of alterations found in the zebrafish liver.

Treatment	Tissue alterations						
	Pyknosis	Leukocyte infiltration	Fatty degeneration	Diffuse congestion	Sinusoidal dilatation	Vacuolization	%P
A		X					16.66%
B		X					16.66%
C	X	X	X	X			66.66%
D	X				X	X	50%
E		X	X	X	X	X	83.33%
F	X	X	X		X		66.66%
G	X	X		X	X		66.66%
H		X		X	X	X	66.66%
I		X	X	X	X	X	83.33%
J	X	X	X		X	X	83.33%
K		X			X	X	50%
L	X	X	X	X		X	83.33%
M	X	X		X	X	X	83.33%
N	X	X	X	X		X	83.33%
O	X	X		X	X	X	83.33%
P	X	X	X	X	X	X	100%

response was not as high as the one produced by compounds alone. The toxic excitatory effect might explain this phenomenon. Several authors, for instance, have posited that the enzymatic activities of SOD and CAT can exhibit an elevation in response to stressors imposed on organisms (Colín-García et al., 2023; Lee et al., 2023; Gutiérrez-Noya et al., 2023). However, when the stress response exceeds a defined threshold, it can suppress antioxidant enzyme activities and modulate the metabolism of reactive oxygen species (ROS) in fish (Elizalde-Velázquez et al., 2022a). Beyond the observed excitatory effect, it is also conceivable that antagonistic interactions transpired within tertiary mixtures, given the discernible increase in levels of oxidative damage biomarkers in mixtures DPM1 to DPM5, comparable to that induced by individual pharmacological agents. This assumption is grounded in antecedent research, which indicates that metformin (MET) may manifest hormetic effects (Elizalde-Velázquez et al., 2021), demonstrate antioxidant activity (Tripathi et al., 2022), and act as an antagonist when used with other pharmaceutical compounds (Godoy et al., 2019). The latter effect, for example, was observed when Danio rerio fish were exposed to MET and bisoprolol or sotalol. Regrettably, further investigation is imperative to elucidate the dynamics of mixtures incorporating MET comprehensively.

A consequence of the oxidative stress induced by individual drugs or their combination is apoptosis, or programmed cell death, attributed to the detrimental impact of ROS on cellular biomolecules. (Checa and Aran, 2020). Nevertheless, it is also accurate that drug-induced ROS can trigger a cascade of responses over various pathways, ultimately leading to an apoptotic response. For example, the ROS produced by N-acetyl-p-benzoquinone imine (NAPQI), a metabolite of PCM, can induce the opening of the mitochondrial permeability transition pore. Consequently, mitochondrial proteins such as apoptosis-inducing factor (AIF) and Endo G relocate to the nucleus, resulting in nuclear DNA fragmentation and ultimately leading to cell death (Yan et al., 2018). Furthermore, the ROS generated by NAPQI can activate the c-Jun N-terminal kinase (JNK) signaling pathways, promoting sustained JNK activity. The

Table 4
Drug quantification in *Danio rerio* liver.

	Nominal Concentrations	Drug quantification		
		DEX (ng/g)	PCM (ng/g)	MET (ng/g)
COTROL	ND	<LOQ	<LOQ	<LOQ
DMSO 0.01%	ND	<LOQ	<LOQ	<LOQ
DEX1	30 ng/L	0.41 ± 0.08	<LOQ	<LOQ
DEX2	60 ng/L	0.87 ± 0.11	<LOQ	<LOQ
PCM1	0.250 μg/L	<LOQ	8.77 ± 0.78	<LOQ
PCM2	0.500 μg/L	<LOQ	13.91 ± 0.59	<LOQ
MET1	20 μg/L	<LOQ	<LOQ	318.42 ± 2.45
MET2	40 μg/L	<LOQ	<LOQ	519.50 ± 3.98
DPM1	30 ng/L + 0.250 μg/L + 20 μg/L	0.39 ± 0.05	8.09 ± 0.34	310.06 ± 3.02
DPM2	60 ng/L + 0.250 μg/L + 20 μg/L	0.81 ± 0.09	8.11 ± 0.72	309.54 ± 1.14
DPM3	30 ng/L + 0.250 μg/L + 40 μg/L	0.40 ± 0.01	7.94 ± 0.41	503.02 ± 4.55
DPM4	60 ng/L + 0.250 μg/L + 40 μg/L	0.83 ± 0.10	8.01 ± 0.68	502.84 ± 3.73
DPM5	30 ng/L + 0.500 μg/L + 20 μg/L	0.31 ± 0.02	14.01 ± 0.94	301.29 ± 4.01
DPM6	60 ng/L + 0.500 μg/L + 20 μg/L	0.74 ± 0.06	14.18 ± 0.21	302.01 ± 2.19
DPM7	30 ng/L + 0.500 μg/L + 40 μg/L	0.32 ± 0.07	14.07 ± 0.49	507.44 ± 2.76
DPM8	60 ng/L + 0.500 μg/L + 40 μg/L	0.77 ± 0.03	13.99 ± 0.89	506.98 ± 4.50

Values are the mean of three replicates ± S.D. LOQ-DEX: 0.45 ng/g. LOQ-PCM: 2.08 ng/g. LOQ-MET: 1.10 ng/g.

above, in turn, amplifies mitochondrial ROS levels, intensifies cellular stress, and exacerbates apoptotic processes (Tashiro et al., 2022). A comparable scenario occurs for MET and DEX, wherein ROS induction, initiated by elevated intracellular calcium levels or mitochondrial complex I inhibition (Elizalde-Velázquez et al., 2022b; Gutiérrez-Noya et al., 2023), results in mitochondrial impairment. After this impairment, a sequential series of events ensues, including initiating the JNK pathway and the liberation of cytochrome C, culminating in cellular apoptosis (Chen et al., 2020; Li et al., 2020). The above is notorious as MET, DEX, PCM, and their mixtures substantially up-regulated the expression of bax, *bcl2*, and *p53*. *bcl2* and *bax* are the bcl-2 protein family's constituents governing the intrinsic apoptosis pathway. More precisely, *bcl2* is an anti-apoptotic protein, exerting its function by impeding the liberation of pro-apoptotic factors from the mitochondria (Qian et al., 2022). Conversely, *bax* operates as a pro-apoptotic protein, instigating cell death through the induction of mitochondrial outer membrane permeabilization (MOMP), which culminates in the discharge of cytochrome *c* and additional apoptotic factors (Dewson and Kluck, 2009; Kuwana et al., 2020). Likewise, *p53* functions as a tumor suppressor protein, regulating the cell cycle. It accomplishes this by imposing a temporary arrest at the G1 phase to facilitate DNA repair or, in cases of irreparable damage, by instigating apoptosis as a mechanism to eliminate compromised cells (Chen, 2016; Wang et al., 2022).

Even though there was an overexpression of apoptotic-related genes in Danio rerio liver across all treatments, our histopathological observations did not show an apoptotic or inflammatory response. The sole tissue modifications noted encompassed pyknosis, leukocyte infiltration, fatty degeneration, diffuse congestion, sinusoidal dilation, and vacuolization, aligning with findings from prior studies. For example, in the histopathological examination conducted by Guiloski et al. (2017), it was observed that male Rhamdia quelen fish, exposed to 2.5 μg/L of PCM for 21 days, displayed mild blood congestion and leukocytic infiltration in the liver. Similarly, Elizalde-Velázquez et al., 2022c documented hepatic alterations in *Danio rerio* following a 96-h exposure to PCM concentrations of 0.125, 0.250, and 0.500 μg/L. These alterations encompassed congestion, hyperemia, infiltration, sinusoidal dilation, macrovascular fat degeneration, and pyknotic nuclei. Regarding DEX, as documented by Zhong et al. (2021), it was noted that following a 60-day exposure period, concentrations of 0.5 and 5 μg/L led to vacuolization in the liver of mosquito fish. Conversely, a concentration of 50 μg/L produced a more severe range of effects, including vacuolization, dilated hepatocytes, hepatocellular degeneration, focal necrosis, and karyopyknosis. Finally, in the investigation conducted by Barbieri et al. (2022), vacuolization was documented at concentrations of 50 μg/L, 100 μg/L, and 1 mg/L in the context of MET exposure. Notably, in the cohort subjected to a concentration of 10 mg/L, notable alterations, including bleeding, edema, and vacuolization, were discerned in the gills of Astyanax lacustris following a 90-day exposure period. From above, it is essential to note that the alterations found are reversible, meaning they have minimal pathological significance. The above implies that the tissue returns to its normal state once exposure to irritants concludes or when the stressing factor is neutralized (Bernet et al., 1999). Nevertheless, in the case of the mixture, there is a belief that prolonged exposure could induce more substantial alterations in the structures of hepatocytes.

5. Conclusions

Short-term exposure to three commonly used COVID-19 medications (MET, DEX, and PCM), both independently and in combination, elicited a notable toxic reaction marked primarily by oxidative harm and increased expression of genes associated with apoptosis. Nevertheless, it is crucial to highlight the presence of hormetic, antagonistic, or antioxidant effects in the combinations, as certain mixtures (DPM1 to DPM5) exhibited a response similar to that induced by individual drugs. Additional research is required to fully elucidate the mechanism through which these mixtures fail to display a heightened response in comparison to individual drugs. Regarding histological observations, our findings indicate that both individual drugs and their combinations do not manifest any tissue alterations that threaten the fish's overall well-being. However, it is hypothesized that prolonged exposure may amplify the toxic response in the liver, leading to increased tissue damage in the hepatocytes. Subsequent investigations should undertake comprehensive studies involving the exposure of organisms to mixtures and under different times of exposure to enhance our understanding of the impact of these combinations on aquatic organisms.

CRediT authorship contribution statement

Diana Belen Onofre-Camarena: Methodology, Investigation, Data curation. **Gustavo Axel Elizalde-Velázquez:** Writing – original draft, Visualization, Supervision, Software, Methodology, Investigation, Formal analysis, Conceptualization. **Leobardo Manuel Gómez-Oliván:** Writing – review & editing, Writing – original draft, Validation, Supervision, Resources, Project administration, Investigation, Funding acquisition, Formal analysis, Conceptualization. **Sandra García-Medina:** Software, Formal analysis, Data curation. **Marcela Galar-Martínez:** Writing – original draft, Supervision, Software. **José Roberto Jerónimo Juárez:** Methodology, Investigation, Data curation. **Selene Elizabeth Herrera-Vázquez:** Visualization, Investigation, Formal analysis, Data curation.

Declaration of competing interest

The authors declare that they have no known competing financial interests or personal relationships that could have appeared to influence the work reported in this paper.

Data availability

Data will be made available on request.

Acknowledgments

This study was made possible by financial support the Consejo Nacional de Ciencia y Tecnología (CONACyt, Project 300727).

Appendix A. Supplementary data

Supplementary data to this article can be found online at https://doi.org/10.1016/j.envpol.2024.123997.

References

Abdallah, M.A.E., Nguyen, K.H., Ebele, A.J., Atia, N.N., Ali, H.R.H., Harrad, S., 2019. A single run, rapid polarity switching method for determination of 30 pharmaceuticals and personal care products in waste water using Q-Exactive Orbitrap high resolution accurate mass spectrometry. J. Chromatogr. A 1588, 68–76.

Ala, M., Ala, M., 2021. Metformin for cardiovascular protection, inflammatory bowel disease, osteoporosis, periodontitis, polycystic ovarian syndrome, neurodegeneration, cancer, inflammation and senescence: what is next? ACS Pharmacol. Transl. Sci. 4 (6), 1747–1770.

Angeles, L.F., Islam, S., Aldstadt, J., Saqeeb, K.N., Alam, M., Khan, M.A., et al., 2020. Retrospective suspect screening reveals previously ignored antibiotics, antifungal compounds, and metabolites in Bangladesh surface waters. Sci. Total Environ. 712, 136285.

aus der Beek, T., Weber, F.A., Bergmann, A., Hickmann, S., Ebert, I., Hein, A., Küster, A., 2016 Apr. Pharmaceuticals in the environment–Global occurrences and perspectives. Environ Toxicol Chem. 35 (4), 823–835. https://doi.org/10.1002/etc.3339. Epub 2016 Feb 25. PMID: 26666847.

Barbieri, P.A., Mari-Ribeiro, I.P., Lupepsa, L., Gigliolli, A.A.S., Paupitz, B.R., de Melo, R. F., et al., 2022. Metformin-induced alterations in gills of the freshwater fish Astyanax lacustris (Lütken, 1875) detected by histological and scanning electron microscopy. Ecotoxicology 31 (8), 1205–1216.

Bradford, M.M., 1976. A rapid and sensitive method for the quantitation of microgram quantities of protein utilizing the principle of protein-dye binding. Anal. Biochem. 72 (1–2), 248–254.

Buege, J.A., Aust, S.D., 1978. [30] Microsomal lipid peroxidation. In: Methods in Enzymology, vol. 52. Academic press, pp. 302–310.

Burns, E.E., Carter, L.J., Kolpin, D.W., Thomas-Oates, J., Boxall, A.B., 2018. Temporal and spatial variation in pharmaceutical concentrations in an urban river system. Water Res. 137, 72–85.

Checa, J., Aran, J.M., 2020. Reactive oxygen species: drivers of physiological and pathological processes. J. Inflamm. Res. 1057–1073.

Chen, C., Yang, J.S., Lu, C.C., Chiu, Y.J., Chen, H.C., Chung, M.I., et al., 2020. Effect of quercetin on dexamethasone-induced C2C12 skeletal muscle cell injury. Molecules 25 (14), 3267.

Chen, J., 2016. The cell-cycle arrest and apoptotic functions of p53 in tumor initiation and progression. Cold Spring Harbor perspectives in medicine 6 (3), a026104.

Colín-García, K., Elizalde-Velázquez, G.A., Gómez-Oliván, L.M., García-Medina, S., 2023. Influence of sucralose, acesulfame-k, and their mixture on brain's fish: a study of behavior, oxidative damage, and acetylcholinesterase activity in Danio rerio. Chemosphere 340, 139928.

Desgens-Martin, V., Keller, A.A., 2021. COVID-19 treatment agents: do they pose an environmental risk? ACS Es&t Water 1 (7), 1555–1565.

Dewson, G., Kluck, R.M., 2009. Mechanisms by which Bak and Bax permeabilise mitochondria during apoptosis. J. Cell Sci. 122 (16), 2801–2808.

Elizalde-Velázquez, G.A., Gómez-Oliván, L.M., García-Medina, S., Rosales-Pérez, K.E., Orozco-Hernández, J.M., Islas-Flores, H., et al., 2022b. Chronic exposure to realistic concentrations of metformin prompts a neurotoxic response in Danio rerio adults. Sci. Total Environ. 849, 157888.

Elizalde-Velázquez, G.A., Gómez-Oliván, L.M., García-Medina, S., Islas-Flores, H., Hernández-Navarro, M.D., Galar-Martínez, M., 2021. Antidiabetic drug metformin disrupts the embryogenesis in zebrafish through an oxidative stress mechanism. Chemosphere 285, 131213.

Elizalde-Velázquez, G.A., Gómez-Oliván, L.M., García-Medina, S., Hernández-Díaz, M., Islas-Flores, H., Galar-Martínez, M., et al., 2022a. Polystyrene microplastics mitigate the embryotoxic damage of metformin and guanylurea in Danio rerio. Sci. Total Environ. 852, 158503.

Elizalde-Velázquez, G.A., Herrera-Vázquez, S.E., Gómez-Oliván, L.M., García-Medina, S., 2023. Health impact assessment after Danio rerio long-term exposure to environmentally relevant concentrations of metformin and guanylurea. Chemosphere 341, 140070.

Elizalde-Velázquez, G.A., Rosas-Ramírez, J.R., Raldua, D., García-Medina, S., Orozco-Hernández, J.M., Rosales-Pérez, K., et al., 2022c. Low concentrations of ciprofloxacin alone and in combination with paracetamol induce oxidative stress, upregulation of apoptotic-related genes, histological alterations in the liver, and genotoxicity in Danio rerio. Chemosphere 294, 133667.

Godoy, A.A., de Oliveira, Á.C., Silva, J.G.M., de Jesus Azevedo, C.C., Domingues, I., Nogueira, A.J.A., Kummrow, F., 2019. Single and mixture toxicity of four pharmaceuticals of environmental concern to aquatic organisms, including a behavioral assessment. Chemosphere 235, 373–382.

Gong, J., Lin, C., Xiong, X., Chen, D., Chen, Y., Zhou, Y., et al., 2019. Occurrence, distribution, and potential risks of environmental corticosteroids in surface waters from the Pearl River Delta, South China. Environ. Pollut. 251, 102–109.

Graham, G.G., Davies, M.J., Day, R.O., Mohamudally, A., Scott, K.F., 2013. The modern pharmacology of paracetamol: therapeutic actions, mechanism of action, metabolism, toxicity and recent pharmacological findings. Inflammopharmacology 21, 201–232.

Greenham, R.T., Miller, K.Y., Tong, A., 2019. Removal efficiencies of top-used pharmaceuticals at sewage treatment plants with various technologies. J. Environ. Chem. Eng. 7 (5), 103294.

Guiloski, I.C., Ribas, J.L.C., Piancini, L.D.S., Dagostim, A.C., Cirio, S.M., Fávaro, L.F., et al., 2017. Paracetamol causes endocrine disruption and hepatotoxicity in male fish Rhamdia quelen after subchronic exposure. Environ. Toxicol. Pharmacol. 53, 111–120.

Gutiérrez-Noya, V.M., Gómez-Oliván, L.M., Casas-Hinojosa, I., García-Medina, S., Rosales-Pérez, K.E., Orozco-Hernández, J.M., et al., 2023. Short-term exposure to dexamethasone at environmentally relevant concentrations impairs embryonic development in Cyprinus carpio: Bioconcentration and alteration of oxidative stress-related gene expression patterns. Sci. Total Environ. 898, 165528.

Hayden, K.R., Jones, M., Elkin, K.R., Shreve, M.J., Clees, W.I., Clark, S., et al., 2022. Impacts of the COVID-19 pandemic on pharmaceuticals in wastewater treated for beneficial reuse: two case studies in central Pennsylvania, 51 (5), 1066–1082.

Jacob, S., Dötsch, A., Knoll, S., Köhler, H.R., Rogall, E., Stoll, D., et al., 2018. Does the antidiabetic drug metformin affect embryo development and the health of brown trout (Salmo trutta f. fario)? Environ. Sci. Eur. 30, 1–16.

Jiang, Z.Y., Hunt, J.V., Wolff, S.P., 1992. Ferrous ion oxidation in the presence of xylenol orange for detection of lipid hydroperoxide in low density lipoprotein. Anal. Biochem. 202 (2), 384–389.

Kuwana, T., King, L.E., Cosentino, K., Suess, J., Garcia-Saez, A.J., Gilmore, A.P., Newmeyer, D.D., 2020. Mitochondrial residence of the apoptosis inducer BAX is more important than BAX oligomerization in promoting membrane permeabilization. J. Biol. Chem. 295 (6), 1623–1636.

Lee, J.H., Kang, J.C., Kim, J.H., 2023. Toxic effects of microplastic (Polyethylene) on fish: accumulation, hematological parameters and antioxidant responses in Korean Bullhead, Pseudobagrus fulvidraco. Sci. Total Environ. 877, 162874.

Levine, R.L., Williams, J.A., Stadtman, E.P., Shacter, E., 1994. [37] Carbonyl assays for determination of oxidatively modified proteins. In: Methods in Enzymology, vol. 233. Academic press, pp. 346–357.

Li, B., Zhou, P., Xu, K., Chen, T., Jiao, J., Wei, H., et al., 2020. Metformin induces cell cycle arrest, apoptosis and autophagy through ROS/JNK signaling pathway in human osteosarcoma. Int. J. Biol. Sci. 16 (1), 74.

Liu, Z.H., Ma, Q.G., Dai, L., Dang, Z., 2023. Occurrence, removal and risk evaluation of ibuprofen and acetaminophen in municipal wastewater treatment plants: a critical review. Sci. Total Environ., 164600

Lukito, A.A., Pranata, R., Henrina, J., Lim, M.A., Lawrensia, S., Suastika, K., 2020. The effect of metformin consumption on mortality in hospitalized COVID-19 patients: a systematic review and meta-analysis. Diabetes & Metabolic Syndrome: Clinical Research & Reviews 14 (6), 2177–2183.

Mastrángelo, M.M., Valdés, M.E., Eissa, B., Ossana, N.A., Barceló, D., Sabater, S., et al., 2022. Occurrence and accumulation of pharmaceutical products in water and biota of urban lowland rivers. Sci. Total Environ. 828, 154303.

Micallef, J., Soeiro, T., Jonville-Bera, A.P., of Pharmacology, F.S., 2020. Non-steroidal anti-inflammatory drugs, pharmacology, and COVID-19 infection. Therapie (Paris) 75 (4), 355–362.

Misra, H.P., Fridovich, I., 1972. The role of superoxide anion in the autoxidation of epinephrine and a simple assay for superoxide dismutase. J. Biol. Chem. 247 (10), 3170–3175.

Perussolo, M.C., Guiloski, I.C., Lirola, J.R., Fockink, D.H., Corso, C.R., Bozza, D.C., et al., 2019. Integrated biomarker response index to assess toxic effects of environmentally relevant concentrations of paracetamol in a neotropical catfish (Rhamdia quelen). Ecotoxicol. Environ. Saf. 182, 109438.

Pes, K., Ortiz-Delgado, J.B., Sarasquete, C., Laize, V., Fernandez, I., 2022. Short-term exposure to pharmaceuticals negatively impacts marine flatfish species: histological, biochemical and molecular clues for an integrated ecosystem risk assessment. Environ. Toxicol. Pharmacol. 90, 103822.

Praveena, S.M., Shaifuddin, S.N.M., Sukiman, S., Nasir, F.A.M., Hanafi, Z., Kamarudin, N., et al., 2018. Pharmaceuticals residues in selected tropical surface water bodies from Selangor (Malaysia): occurrence and potential risk assessments. Sci. Total Environ. 642, 230–240.

Pulicharla, R., Proulx, F., Behmel, S., Sérodes, J.B., Rodriguez, M.J., 2021. Occurrence and seasonality of raw and drinking water contaminants of emerging interest in five water facilities. Sci. Total Environ. 751, 141748.

Qian, S., Wei, Z., Yang, W., Huang, J., Yang, Y., Wang, J., 2022. The role of BCL-2 family proteins in regulating apoptosis and cancer therapy. Front. Oncol. 12, 985363.

Radi, R., Turrens, J.F., Chang, L.Y., Bush, K.M., Crapo, J.D., Freeman, B.A., 1991. Detection of catalase in rat heart mitochondria. J. Biol. Chem. 266 (32), 22028–22034.

RECOVERY Collaborative Group, 2021. Dexamethasone in hospitalized patients with Covid-19. N. Engl. J. Med. 384 (8), 693–704.

Rivera-Jaimes, J.A., Postigo, C., Melgoza-Alemán, R.M., Aceña, J., Barceló, D., de Alda, M.L., 2018. Study of pharmaceuticals in surface and wastewater from

Cuernavaca, Morelos, Mexico: occurrence and environmental risk assessment. Sci. Total Environ. 613, 1263–1274.
Rosas-Ramírez, J.R., Orozco-Hernández, J.M., Elizalde-Velázquez, G.A., Raldúa, D., Islas-Flores, H., Gómez-Oliván, L.M., 2022. Teratogenic effects induced by paracetamol, ciprofloxacin, and their mixture on Danio rerio embryos: oxidative stress implications. Sci. Total Environ. 806, 150541.
Sharma, M., Verma, S., Sharma, P., 2019. Behavioural and genotoxic effects of paracetamol after subchronic exposure to Cyprinus carpio. J Entomol Zool Stud 7 (3), 22–25.
Shen, X., Chang, H., Sun, Y., Wan, Y., 2020. Determination and occurrence of natural and synthetic glucocorticoids in surface waters. Environ. Int. 134, 105278.
Stasi, C., Fallani, S., Voller, F., Silvestri, C., 2020. Treatment for COVID-19: an overview. Eur. J. Pharmacol. 889, 173644.
Tashiro, S., Tanaka, M., Goya, T., Aoyagi, T., Kurokawa, M., Imoto, K., et al., 2022. Pirfenidone attenuates acetaminophen-induced liver injury via suppressing c-Jun N-terminal kinase phosphorylation. Toxicol. Appl. Pharmacol. 434, 115817.
Tripathi, S.S., Singh, S., Garg, G., Kumar, R., Verma, A.K., Singh, A.K., et al., 2022. Metformin ameliorates acetaminophen-induced sub-acute toxicity via antioxidant property. Drug Chem. Toxicol. 45 (1), 52–60.
Wang, Y.H., Ho, T.L., Hariharan, A., Goh, H.C., Wong, Y.L., Verkaik, N.S., et al., 2022. Rapid recruitment of p53 to DNA damage sites directs DNA repair choice and integrity. Proc. Natl. Acad. Sci. USA 119 (10), e2113233119.
Wilkinson, J.L., Boxall, A.B., Kolpin, D.W., Leung, K.M., Lai, R.W., Galbán-Malagón, C., et al., 2022. Pharmaceutical pollution of the world's rivers. Proc. Natl. Acad. Sci. USA 119 (8), e2113947119.
Yan, M., Huo, Y., Yin, S., Hu, H., 2018. Mechanisms of acetaminophen-induced liver injury and its implications for therapeutic interventions. Redox Biol. 17, 274–283.
Zhang, R., He, Y., Yao, L., Chen, J., Zhu, S., Rao, X., et al., 2021. Metformin chlorination byproducts in drinking water exhibit marked toxicities of a potential health concern. Environ. Int. 146, 106244.
Zhong, L., Liang, Y.Q., Lu, M., Pan, C.G., Dong, Z., Zhao, H., et al., 2021. Effects of dexamethasone on the morphology, gene expression and hepatic histology in adult female mosquitofish (Gambusia affinis). Chemosphere 274, 129797.